Morphology of a solidifying interface near a spherical particle: Disjoining pressure effects

L. Hadji*
Mathematics Department, The University of Alabama, Tuscaloosa, Alabama 35487-0350
(Received 30 August 2001; published 23 January 2002)

Numerical simulations were conducted to determine the morphology of a solid-liquid interface near an insoluble spherical particle. The model accounts for the undercoolings due to the front's curvature and to the nonretarded van der Waals interactions. Our numerical results show that, in the near-contact region, the interface profile develops a sharp peak whose curvature has a logarithmic singularity. This is in agreement with the asymptotic analysis of a previously published equation for the interface profile.

DOI: 10.1103/PhysRevE.65.022201 PACS number(s): 64.70.Dv, 81.30.Fb, 81.05.Ni

I. INTRODUCTION

In this paper we focus on the analysis of the shape of an advancing solid-liquid interface as it approaches a neutrally buoyant particle. The analysis pertains to the case of a solid front whose deformations are induced solely by its interaction with the particle. Our interest in this problem has been largely motivated by applications in the fabrication of particulate metal matrix composites [1,2]. For a general review of the problem, we refer the reader to Refs. [3–5]. It is well known that the presence of a foreign particle near a solid-liquid interface modifies locally the melting point of the substance. The change in the melting point is due to several factors, such as the difference in thermal conductivities of the particle and melt, the disjoining pressure and the hydrodynamic pressure that arise in the melt film separating the interface from the particle's surface. The quantification of the front's deformation in terms of the material and processing properties is essential to the understanding of the interaction of inclusions in the melt with a solidifying interface. The dependence of the interface morphology on the physical and processing parameters has not been fully resolved and its determination remains an intensive area of research.

Two lines of inquiry are considered here: (i) the numerical investigation of the morphology of the interface near a foreign particle when the undercooling due to the disjoining pressure is the sole cause of interfacial distortion, (ii) comparison of the numerics with the predictions of a previously published asymptotic analysis of the same problem [6].

II. NUMERICAL ANALYSIS OF THE INTERFACE PROFILE

Consider a spherical particle of radius a that is placed in the melt a distance h_∞ from the planar solid-liquid interface as illustrated in the schematic diagram shown in Fig. 1.

On using an axisymmetric setup with the vertical coordinate z and radial coordinate r, taken along the solid-liquid (S/L) interface, the particle-liquid boundary is given by

$$[z-(a+h_\infty)]^2+r^2=a^2. \tag{1}$$

Assume that the coefficients of thermal conductivity of the particle and the melt are equal. Then the thermal field is given by

$$T(r,z)=T_m+Gz, \tag{2}$$

where T_m is the melting point of the pure substance and G is the externally imposed thermal gradient. Under the assumption that only the undercoolings due to the disjoining pressure and front's curvature are accounted for, the equilibrium temperature of the solid-liquid interface is given by [3]

$$T_{\rm int}=T_m+\Delta T_{\rm curv}+\Delta T_{\rm dp}, \tag{3}$$

where $\Delta T_{\rm curv}$ is the curvature undercooling given by the Gibbs-Thomson formula [7],

$$\Delta T_{\rm curv}=-\frac{\sigma_{S/L}T_m}{L}\mathcal{K}, \tag{4}$$

and $\Delta T_{\rm dp}$ is the undercooling due to the disjoining pressure, $\mathcal{P}_{\rm dp}=\mathcal{A}/6\pi g^3$, and given by [3,8],

$$\Delta T_{\rm dp}=\frac{\mathcal{A}T_m}{6\pi L g^3(r)}. \tag{5}$$

Equation (5) is also referred to as a Derjaguin approximation [9]. The symbols that appear in the above equations are defined as follows: $\sigma_{S/L}$ is the surface excess free energy in solid-liquid interface, L is the latent heat of fusion per unit

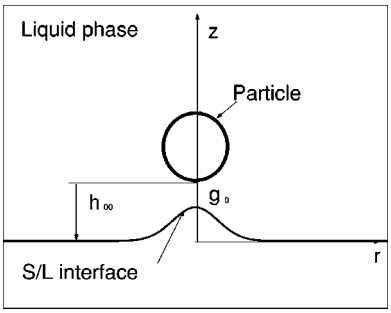

FIG. 1. Sketch of a particle of radius a near a deformed S/L interface, g_0 is the gap thickness at the origin, $r=0$ and h_∞ is the distance between the lowest point on the particle's surface and the undisturbed planar S/L interface.

*Email address: lhadji@bama.ua.edu

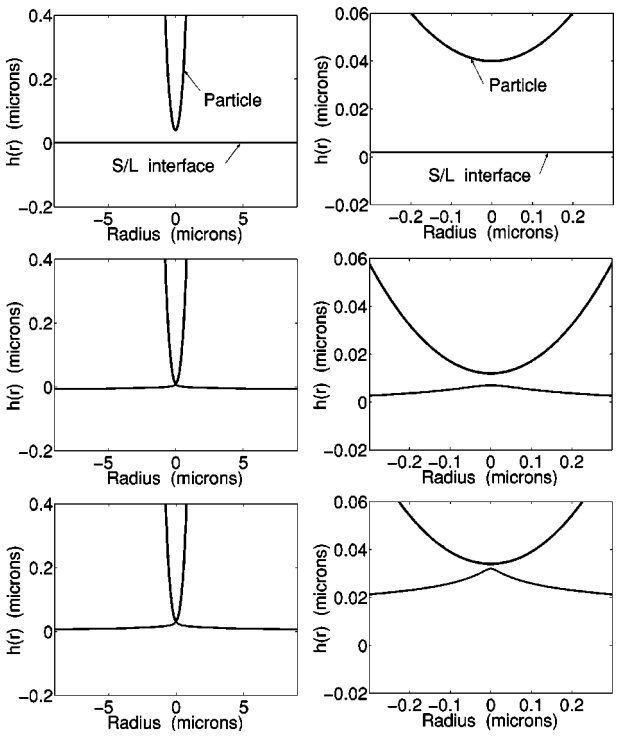

FIG. 2. Plot of $h(r)$ for the case $\mathcal{A}>0$ for three values of the gap separation $g_0=380$ (top set), 50 (middle set), and 20 Å (bottom set). The figure on the left side depicts the positions of the particle and interface over a horizontal extent of five particle diameters while the corresponding figures on the right side are magnifications of the near-contact region.

volume, $\mathcal{A}$ is the Hamaker constant whose sign is positive when $\mathcal{P}_{\rm dp}$ increases as the gap thickness $g(r)$ grows small. The width of the gap separating the particle from the lower half of the particle is given by $g(r)=[h_\infty+a-\sqrt{|a^2-r^2|}-h(r)]$ where $h(r)$ is the interface profile. The front's curvature, which is taken to be positive when the center of curvature lies in the solid phase, is given by

$$\mathcal{K}=-\frac{h''(r)}{[1+(h')^2]^{3/2}}-\frac{h'(r)}{r[1+(h')^2]^{1/2}}. \tag{6}$$

The interface temperature is obtained upon evaluating Eq. (2) at $z=0$, and on using Eq. (3), a differential equation for the interface curvature is obtained, namely,

$$\mathcal{K}=\frac{\mathcal{A}}{6\pi\sigma_{S/L}}g^{-3}(r). \tag{7}$$

The following system of two first order differential equations for the interface profile results upon equating Eqs. (6) and (7),

$$\frac{dh}{dr}=v(r),$$

$$\frac{dv}{dr}=(1+v^2)^{3/2}\left[-\frac{v}{r}(1+v^2)^{-1/2}-\frac{\mathcal{A}}{6\pi\sigma_{S/L}}\frac{u(a-r)}{g^3(r)}\right], \tag{8}$$

where the unit step function $u(a-r)$ is used to model the fact that the disjoining pressure acts only in the melt film between the particle and the crystal. The above equations are complemented by the following conditions: (i) the symmetry condition $v(0)=0$ and (ii) far away from the particle, the interface is not affected by the particle's presence and so it remains planar, i.e., $h(r)\to 0$ as $r\to\infty$. Therefore, the determination of the interface profile requires solving the boundary value problem (8). We have undertaken the solution of Eq. (8) as an initial value problem by making use of an assumed value for the profile's location at $r=0$ and of the symmetry condition $v(0)=0$; the correct value for $h(0)$, within discretization error, is the one that causes $h(r)$ to vanish far away from the particle (taken here to mean five particle diameters). We circumvent evaluating Eq. (8) at the origin by the following procedure: at the origin $r=0$, we have $dv/dr=-\mathcal{A}/6\pi\sigma_{S/L}[h_\infty-h(0)]^3$ since $v(0)=0$. On using a forward difference formula for dv/dr, we obtain the value of v to the right of zero as, $v(\delta)=-\delta\mathcal{A}/6\pi\sigma_{S/L}[h_\infty-h(0)]^3$ where we have set $\delta=10^{-15}$. For $r>\delta$, Eqs. (8) are solved using the Matlab numerical routine ODE45.

We consider the numerical solution of Eq. (8) for an experimental system consisting of the transparent organic material Succinonitrile immersed with Polystyrene particles (SCN-PS). We have obtained the numerical values of the constants from Ref. [2]. They are $T_m=328$ K, $L=4.6\times10^7$ J/m^3, $\sigma_{S/L}=0.03$ J/m^2. As for the Hamaker constant, we have arbitrarily used $\mathcal{A}=\pm10^{-19}$ J. This numerical value of $\mathcal{A}$ is typical for liquid films for which the disjoining pressure results from the nonretarded van der Waals interactions. We have investigated the change in the morphology of the solid-liquid interface as it approaches the particle. Figure 2 depicts the profiles $h(r)$ for a particle radius $a=1$ μm and for three distinct values of the gap separation, $g_0=h_\infty-h(0)$. A shooting strategy is used to determine the initial value $h(0)$ that makes the profile vanish at a distance $10a$ from the origin while h_∞ is chosen arbitrarily and represents the distance from the planar interface to the lowest point on the particle's surface; the parameter h_∞ quantifies the position of the particle with respect to the interface. The values of $h(0)$ and h_∞ used in these runs are 20 and 400 Å for the top plots, 70 and 120 Å for the middle plots, and 320 and 340 Å for the bottom plots. These correspond to gap thicknesses 380, 50, and 20 Å, respectively. Notice the dramatic change in the interface shape as the gap separation is decreased. The bottom plot, which depicts an ultrathin gap separation, shows an interface that has acquired a cusplike shape while the amount of interfacial distortion is about 300 Å. The ratio of the amount of interface distortion to the particle's radius is about 0.03. These runs reveal an important piece of information, namely, the very near proximity of the particle to the crystal is associated with the formation of a bump whose curvature is very large. The cause for the large curvature can be traced back to Eq. (7) that depicts a balance between the disjoining pressure $\mathcal{P}_{\rm dp}$ and the pressure change due to the Gibbs-Thomson effect, $\mathcal{P}_{\rm GT}=\sigma_{S/L}\mathcal{K}$. Equation (7) implies that the shape of the solid-liquid interface is deter-

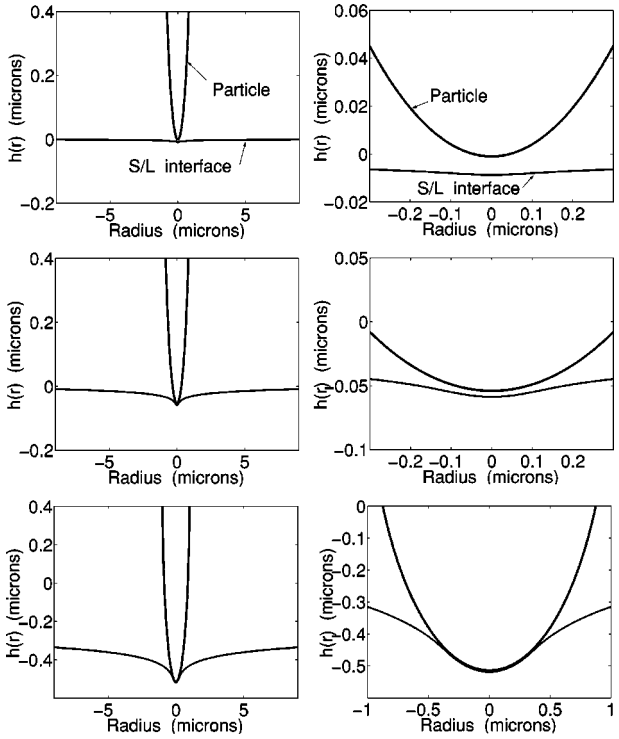

FIG. 3. Plot of $h(r)$ for the case $\mathcal{A}<0$ for three values of the gap separation $g_0=77$ (top set), 47 (middle set), and 44.6 Å (bottom set). The figure on the left side depicts the positions of the particle and interface over a horizontal extent of five particle diameters while the corresponding figures on the right side are magnifications of the near-contact region.

mined by a competition between the disjoining pressure that acts to increase the front's curvature and the Gibbs-Thomson effect that acts to decrease it.

Figure 3 is an illustration of the particle-crystal interaction for a negative Hamaker constant. Three distinct values for h_∞ are considered, namely -10 Å for the top plots, -540 Å for the middle plots, and -5142.4 Å for the bottom plots. These values correspond to the following calculated values of the initial value $h(0)$, -87, -587, and -5187 Å, respectively, and the resulting gap thicknesses g_0 are 77, 47, and 44.6 Å, respectively. Attempts at solving Eq. (8) for a value of h_∞ and corresponding value of $h(0)$ for which the gap thickness g_0 is below 44.6 Å were unsuccessful. The numerical routine is unable to meet the integration tolerances without reducing the step size below the smallest value allowed by the machine. Thus we are unable to confirm the formation of a sharp peak in the front's profile in this case. The simulation runs with macroscopic particles yield patterns similar to those depicted in Figs. 2 and 3.

III. COMPARISON WITH THEORY

An asymptotic analysis of the interface profile near a particle was undertaken by Hadji [6]. He considered a coupled model of fluid flow and heat transfer that also accounts for heat flow in the particle and for the occurrence of interfacial deformations. The particle is assumed to be in near-contact with the front, namely $h=h^*/a\ll 1$, where a is the particle's

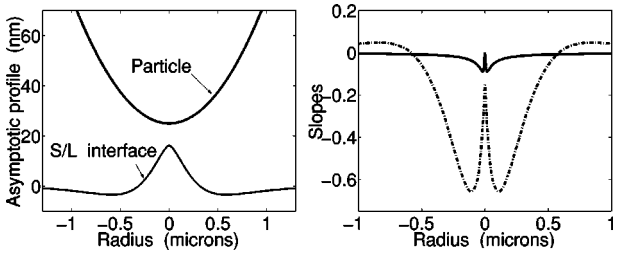

FIG. 4. (left) Plot of the asymptotic profile represented by Eq. (9) in nanometers (nm) for a polystyrene particle of radius $a=1.0$ μm immersed in SCN; (right) plot of the slope of the interface profile $h(r)$ in the near-contact region for a particle radius $a=1.0$ μm and $\mathcal{A}=10^{-19}$ J (continuous line) and the scaled slope of the asymptotic interface profile (dashed-dotted line) with $\epsilon=10^{-3}$.

radius and h^* is the dimensional thickness of the particle-crystal gap. A small perturbation parameter is introduced by setting $h=\epsilon H$ where $H=O(1)$. The analysis assumes the following: (i) the fluid flow motion induced by the particle's movement is small enough to warrant the neglect of the inertia terms in the equations of momentum conservation, (ii) the interface equilibrium temperature accounts for the undercooling terms due to front curvature and disjoining pressure, (iii) the density changes due to changes in temperature are ignored so that the buoyancy term is absent in the momentum equations, (iv) the particle is assumed spherical and neutrally buoyant, and (v) the particle's thermal conductivity is set equal to that of the melt so that no interfacial distortions are caused by thermal effects. The model can easily be extended to include the effects of the hydrodynamic pressure in the melt film that separates the particle from the front. In the case presented here, the fluid flow has no influence on the front's morphology.

The following uniformly valid expression for the interface profile is obtained:

$$\zeta(r)=\frac{\epsilon^3\beta}{h^3G}\left[I_0[r/\sqrt{2\gamma h}^{1/2}]\int_{r/(2\gamma h)^{1/2}}^{\infty}\frac{\xi K_0(\xi)d\xi}{(1+\gamma\xi^2)^3}-K_0(r/\sqrt{2\gamma h})\int_0^{r/\sqrt{2\gamma h}}\frac{\xi I_0(\xi)d\xi}{(1+\gamma\xi^2)^3}\right], \tag{9}$$

where G is the scaled thermal gradient, β is a grouping representing the effect of the disjoining pressure, γ is a grouping representing the surface energy term, r is the radius, and I_0 and K_0 denote the modified Bessel functions of order zero of the first and second kind, respectively. The precise definitions of these dimensionless symbols (see Ref. [6]) are: $\beta=\mathcal{A}/(6\pi La^3)$, $\gamma=\sigma_{S/L}T_m\epsilon/(2a^2LGh)$; ϵ is the perturbation parameter and is of the same order of magnitude as the dimensionless gap separation h. The plot of the asymptotic profile represented by Eq. (9) is shown in Fig. 4 for parameter values corresponding to an SCN-PS experimental system [2]. Note that the front's profile resembles the peak shown in Fig. 2.

To obtain the asymptotic behavior of the interface profile near the origin, it is convenient to let $x=r/\sqrt{2\gamma h}$ and rewrite Eq. (9) as

$$\zeta(x)=\frac{\xi^3\beta}{h^3G}\left[I_0(x)\int_0^{\infty}\frac{\xi K_0(\xi)d\xi}{(1+\gamma\xi^2)^3}-I_0(x)\int_0^{x}\frac{\xi K_0(\xi)d\xi}{(1+\gamma\xi^2)^3}-K_0(x)\int_0^{x}\frac{\xi I_0(\xi)d\xi}{(1+\gamma\xi^2)^3}\right]. \tag{10}$$

We let $\xi=xy$ in the second and third integral terms and on using the facts that $K_0(xy)\sim-\ln(xy)$ and $I_0(xy)\sim 1$ as $x\to 0$ given that $0\leqslant y\leqslant 1$, we have

$$\zeta(x)\sim\frac{\epsilon^3\beta}{h^3G}\left[\int_0^{\infty}\frac{\xi K_0(\xi)d\xi}{(1+\gamma\xi^2)^3}+x^2\int_0^{1}\frac{y(2\ln x+\ln y)dy}{(1+\gamma x^2y^2)^3}\right]. \tag{11}$$

We make use of the fact that $1/(1+\gamma x^2y^2)^3\sim(1-3\gamma x^2y^2)$ given that $x\ll 1$ and $0\leqslant y\leqslant 1$ in the second integral. With $h=\epsilon H$, the evaluation of the resulting expressions yields,

$$\zeta(x)\sim\frac{\beta}{H^3G}\left[\int_0^{\infty}\frac{\xi K_0(\xi)d\xi}{(1+\gamma\xi^2)^3}+x^2\ln x-\frac{x^2}{4}-\frac{3}{2}\gamma x^4\ln x+\cdots\right]\quad\text{as}\quad x\to 0. \tag{12}$$

Upon reverting to the original unscaled variables, Eq. (12) takes the following form for $h(\ll 1)$ fixed,

$$\zeta\left(\frac{r}{(2\gamma h)^{1/2}}\right)\sim\frac{\beta}{H^3G}\left[\int_0^{\infty}\frac{\xi K_0(\xi)d\xi}{(1+\gamma\xi^2)^3}+\frac{r^2}{2\gamma h}\ln\left(\frac{r}{(2\gamma h)^{1/2}}\right)+\cdots\right]\quad\text{as}\quad r\to 0. \tag{13}$$

The first integral term in Eq. (13) satisfies

$$0<\int_0^{\infty}\frac{\xi K_0(\xi)}{(1+\gamma\xi^2)^3}d\xi<1.$$

The presence of the logarithmic term in the expression for $\zeta(r)$ implies a logarithmic singularity in the curvature of the interface profile. In order to compare the predictions of the asymptotic analysis with the numerical results, we have plotted in Fig. 4 the (numerical) slope, $dh/dr=v(r)$, for parameter values that yield a peak in the interface profile similar to that shown in Fig. 2, for a particle radius $a=1.0\ \mu$m and the slope of the asymptotic profile [Eq. (10)]. The fact that both curves exhibit a sharp corner at the origin is an indication of the presence of a singularity in the front's curvature at $r=0$. The asymptotic analysis predicts that the singularity is logarithmic. The experimental testing of the theoretical predictions put forth in this paper will require careful experiments in a microgravity environment to eliminate the possibility of buoyancy-induced flows and gravitational settling of the particle. These effects will normally obscure the observation of the phenomena predicted in this paper. We are aware of one microgravity experiment dealing specifically with the interaction of particles with an advancing solid-liquid interface that was performed recently on the space shuttle Columbia [10]. Unfortunately, the findings are of little relevance to this study given that hardware constraints did not allow for a clear view of the particles near the crystallization front [11].

ACKNOWLEDGMENT

This work was supported by the National Science Foundation through Grant No. DMS-9700380.

[1] A. R. Kennedy and T. W. Clyne, Cast Met. Res. J. **4**, 160 (1991).
[2] D. M. Stefanescu, R. V. Phalnikar, H. Pang, S. Ahuja, and B. K. Dhindaw, ISIJ Int. **35**, 300 (1995).
[3] A. A. Chernov and D. E. Temkin, in *Current Topics in Materials Science*, edited by E. Kaldis and H. J. Scheel (North-Holland, Amsterdam, 1977), Vol. 2. pp. 3–77.
[4] P. K. Rohatgi, R. Asthana, and S. Das, Int. Metall. Rev **31**, 115 (1988).
[5] D. Li and A. W. Neumann, in *Applied Surface Thermodynamics*, edited by A. W. Neumann and Jan K. Spelt (Dekker, New York, 1996), Vol. 63, pp. 557–629.
[6] L. Hadji, Europhys. Lett. **51**, 413 (2000).
[7] W. Kurz and D. J. Fisher, *Fundamentals of Solidification* (Trans. Tech. Pub., Switzerland, 1989).
[8] A. A. Chernov, D. E. Temkin, and A. M. Mel'nikova, Sov. Phys. Crystallogr. **21**, 36 (1976).
[9] J. N. Israelachvili, *Intermolecular and Surface Forces* (Academic, London, 1991).
[10] D. M. Stefanescu, F. R. Juretzko, B. K. Dhindaw, A. Catalina, S. Sen, and P. A. Curreri, Metall Trans. A **29**, 1697 (1998).
[11] D. M. Stefanescu (private communication).